Research Square

Preprints are preliminary reports that have not undergone peer review.
They should not be considered conclusive, used to inform clinical practice,
or referenced by the media as validated information.

Label-free holotomography reveals dynamic structural remodeling in living pancreatic islets

Naoaki Sakata

naoakisakata@fukuoka-u.ac.jp

Fukuoka University https://orcid.org/0000-0002-3495-4270

Ryo Kawakami

https://orcid.org/0000-0002-0525-1189

Teppei Yamada

Gumpei Yoshimatsu

Shohta Kodama

Article

Keywords: Holotomography, Islet, Islet Transplantation, Central Necrosis, Imaging

Posted Date: November 24th, 2026

DOI: https://doi.org/10.21203/rs.3.rs-11445833/v1

License: This work is licensed under a Creative Commons Attribution 4.0 International License.
Read Full License

Additional Declarations: There is **NO** Competing Interest.

Abstract

Dynamic structural changes during pancreatic islet deterioration remain poorly understood. Here, we used label-free holotomography to visualize living murine islets in high-resolution three dimensions and in real time during early culture. Islets were examined after overnight culture at 24°C (Day 0) and after two additional days at either 24°C or 37°C. After overnight culture, holotomography revealed that islets exhibited intercellular dissociation, rupture-like events, and membrane blebbing in both central and peripheral regions. After two additional days at 37°C, holotomography revealed central necrotic remodeling accompanied by extrusion of putative necrotic-core components. Despite greater early structural injury and reduced insulin secretion and content after 14 days, islets cultured at 37°C showed better glycemic control after transplantation than those cultured at 24°C. These findings reveal a divergence between early morphology, later in vitro function, and graft performance at the culture-condition level. Holotomography captures dynamic structural changes in living islets and provides complementary information for assessing islet condition alongside functional and transplantation-based measurements.

Introduction

Pancreatic islet transplantation (ITx) can restore endogenous insulin secretion and improve glycemic control in patients with severe diabetes.[1] It is considered that the therapeutic efficacy of ITx depends critically on the quality and functional reserve of transplanted islets. For example, the oxygen consumption rate of islets and islet equivalents (IEQs) was highly correlated with insulin independence in clinical islet autotransplantation.[2] Furthermore, pretransplant hypoxia worsens the therapeutic effects of transplanted human islets.[3] Therefore, reliable pretransplant assessments of islet condition remain a central challenge in islet biology and transplantation. However, conventional examinations, including glucose-stimulated insulin secretion (GSIS), viability assays, and transplantation using small animal models, have important limitations. GSIS does not always correlate with clinical transplant outcomes.[4, 5] Viability assays often require fluorescent dyes. Furthermore, transplantation using small animals is time-consuming and unsuitable for rapid pretransplant decision-making. Therefore, a simple, non-invasive, and dynamic method for evaluating the condition of living islets is needed.

We consider that morphological assessment is one of the potential strategies for assessing islet condition. Isolated islets undergo structural and cellular changes during culture, and central necrosis is a characteristic feature of damaged or hypoxic islets.[6] This phenomenon is typically observed in large islets, because diffusion constraints and oxygen consumption can create an unfavorable microenvironment within the islet core, leading to apoptosis and necrosis in the central region.[6, 7] These structural abnormalities are expected to influence endocrine function because long-term culture can alter GSIS, insulin content, and endocrine gene expression.[8] Nevertheless, the spatial and temporal sequence by which cell death progresses within living islets remains poorly understood. In particular,

whether islet deterioration reflects simply cell death or a spatially organized process that evolves dynamically during culture remains unclear.

Holotomography is a label-free quantitative phase imaging technology that reconstructs high-resolution three-dimensional images by measuring refractive index (RI) distributions.[9, 10, 11] This modality enables time-lapse imaging of living cells and subcellular structures with low phototoxicity and without exogenous labels.[9, 10, 11] Holotomography has been applied to visualize cellular morphology, organelle dynamics, dry mass, and cell-death-associated features in living cells.[10, 11, 12] We hypothesized that label-free holotomography would allow direct visualization of early, dynamic, and spatially organized morphological changes in living pancreatic islets.

Here, we used label-free holotomography to characterize dynamic intercellular dissociation, rupture-like events, membrane blebbing, and central necrotic remodeling in living murine islets during early culture at 24°C or 37°C. We also assessed insulin secretion, insulin content, gene expression, and transplantation outcomes after prolonged culture to examine how early structural changes relate to later islet function at the culture-condition level.

Results

Label-free holotomography enables real-time visualization of living pancreatic islets beyond conventional bright-field microscopy

Briefly, murine islets were cultured overnight under an atmosphere of 5% CO_2 at 24°C. We defined overnight cultured islets as islets on Day 0. After that, they were cultured in the same medium at 24°C or 37°C for two days. The islets were defined as islets on Day 2 at 24°C and 37°C, respectively. Images of cultured islets (Day 0, Day 2 at 24°C and 37°C) were obtained at ×400 magnification using Z-stack mode on a BZ-X700 microscope (as conventional bright-field microscopy) or HT-X1 system (as label-free holotomography) (Fig. 1A).

Label-free holotomography visualized multiple dynamic subcellular and cellular events in islets, which were not evident by conventional bright-field microscopy. One of the findings was the apparent release of granule-like structures from islet cells. The holotomographic image of an islet on Day 0 is shown in Fig. 1B. Individual endocrine cells contained numerous small high-intensity intracellular granule-like structures. Some of them appeared to be released from islet cells and dispersed into the culture medium over time. These high-intensity islet granules were considered to include putative insulin secretory granules because β cells account for most of the cells in murine islets. Although cell-type-specific identification could not be confirmed by holotomography alone, this interpretation is consistent with islet cellular composition. By contrast, bright-field microscopy time-lapse images did not reveal comparable dynamic changes, although cell-to-cell boundaries could be detected at the same magnification

(Fig. 1C). These findings indicate that label-free holotomography provides substantially richer dynamic information on living islet microarchitecture than conventional bright-field microscopy.

Holotomography reveals early injury-associated morphological events and dynamic loss of intercellular cohesion in Day 0 overnight cultured islets

Before the present study, we expected islets cultured overnight to be morphologically stable. In general, rodent islets have a golden-brown, round shape with a smooth surface without blebbing after culturing for 16–20 h.[13] Consistent with this expectation, conventional bright-field microscopy did not reveal obvious morphological changes in Day 0 islets during 60 min of observation (Fig. 1C).

By contrast, label-free holotomography identified dynamic morphological events in Day 0 islets (Fig. 2). Initially, several cells showed morphological features potentially associated with cellular injury, including non-apoptotic cell death and apoptosis. Figure 2A shows that a peripheral islet cell in islet No. 4 expanded at 14 min and ruptured at 16 min (Fig. 2A and Supplementary Fig. 4). This rupture-like event was morphologically compatible with lytic cell death[14]. Similar rupture-like events were observed in islets Nos. 2 and 3 (Supplementary Figs. 2 and 3 and Video 1). In islet No. 3, a round structure approximately 5 μm in diameter emerged from a ruptured cell at 42 min and subsequently migrated within the field of view (Fig. 2B and Supplementary Fig. 3). Similar findings were seen in islet Nos. 1, 2 and 4 on Day 0 (Supplementary Figs. 1, 2, and 4 and Video 1). This structure was interpreted as a nuclear- or nuclear-remnant-like structure. Plasma membrane rupture and the apparent release of intracellular contents were morphologically consistent with lytic or necrotic cell death rather than classical apoptosis, in which plasma membrane integrity is generally maintained. However, the specific cell-death pathway could not be determined by holotomography alone. Membrane blebbing, a possible morphological feature associated with apoptosis,[15, 16] was also widely observed, including in a peripheral cell of islet No. 5 (Fig. 2C, Supplementary Fig. 5). These observations suggest that both apoptotic-like and non-apoptotic cell-death-like morphological processes can be visualized dynamically in living islets. Furthermore, the signs of both types of cell death were observed not only in the center but also in the peripheral regions of the islets.

A particularly striking finding was the dissociation of intercellular junctions between islet cells. This phenomenon was observed in four of five Day 0 islets and was especially prominent in islet Nos. 2 and 3 (Fig. 2D, Supplementary Figs. 2 and 3 and Video 1). In islet No. 2, dynamic splitting began in the northwest region at 18 min and progressed toward the center, resulting in widespread dissociation of cell-cell contacts. In islet No. 3, multiple cells were dispersed in different directions after junctional dissociation. These observations challenge the assumption that islets cultured overnight are fully morphologically stabilized and indicate that early post-isolation vulnerability of intercellular cohesion can persist even after overnight culture.

We assessed the grayscale intensity (GI) in granule-like structures and in cytoplasm of peripheral and central islet cells. Mean intensities were 174.60 ± 7.72 in granule-like structures, 107.87 ± 6.04 in

cytoplasm of peripheral islet cells and 69.40 ± 5.81 in cytoplasm of central islet cells, respectively. GI differed significantly among the compartments ($p < 0.01$ for peripheral vs. central cytoplasm and $p < 0.0001$ for the other two comparisons; Fig. 2E).

Holotomography reveals temperature-dependent central necrotic remodeling of pancreatic islets

We next assessed Day 2 islets cultured at 24°C or 37°C. Before holotomographic imaging, islet viability was evaluated using Hoechst 33342 / propidium iodide (PI) double staining (Fig. 3A). Most of the Day 2 24°C islets were separated from each other and contained few PI-positive dead cells. By contrast, some Day 2 37°C islets harbored PI-positive cells concentrated in the central region. Viability was significantly lower in Day 2 37°C islets than in Day 2 24°C islets, reflecting central necrosis (92.29 ± 1.18% on Day 2 24°C vs. 80.83 ± 5.57% on Day 2 37°C, $p < 0.01$; Fig. 3B). Histological assessment using islet sections also revealed that some islets on Day 2 37°C contained central necrosis and apoptotic cells (Fig. 3C). The ratio of apoptotic cells per islet was 5.15 ± 1.84% on Day 2 24°C and 8.87 ± 1.46% on Day 2 37°C, respectively (Fig. 3D). The ratio tended to be higher on Day 2 at 37°C, but there was no significant difference. Regarding viability and apoptosis assessments, the number of evaluable islet profiles varied between groups, because the number of islets represented could not be precisely controlled during sample preparation.

Bright-field microscopy showed that Day 2 24°C islets generally retained a round shape with a smooth surface and no obvious central necrosis (Fig. 4A). On Day 2 37°C, central necrosis and central cavity-like structures without cellular components were observed in some islets (Fig. 4A). However, bright-field microscopic time-lapse imaging did not capture dynamic changes during the 60-min observation period. By contrast, holotomography revealed clear temperature-dependent differences in islet remodeling. Day 2 24°C islets showed robust intercellular contacts without the prominent junctional dissociation observed in Day 0 islets (Fig. 4B). These islets also retained abundant high-intensity intracellular granule-like structures, suggesting preservation of granule-rich endocrine cell features under 24°C culture. Only occasional blebbing cells were observed in Day 2 24°C islets (Supplementary Figs. 6–10 and Video 2).

Day 2 37°C islets showed markedly different holotomographic dynamics. In islet No. 2, a low-intensity central region containing dispersed high-intensity granule-like structures was observed, consistent with central necrosis (Fig. 4C and Supplementary Fig. 12 and Video 3). This region appeared to contain fluid- and cellular debris-like components within the central low-intensity region. Extrusion of putative necrotic-core components began at 2 min and continued until 34 min. A similar process was observed in islet No. 4, in which extrusion was present from the beginning of imaging and persisted throughout the observation period (Fig. 4C and Supplementary Fig. 14). Overall, extrusion of central debris-like components was observed in four of five Day 2 37°C islets and in none of the Day 2 24°C islets (Supplementary Figs. 11–14 and Video 3). Islet No.5 did not show extrusion, however, rupture-like events were observed in central cells of the islet (Supplementary Fig. 15). These findings suggest that central

cavity formation is a dynamic remodeling process involving extrusion of core components rather than a static degenerative endpoint.

Finally, we quantified islet cell loss and the intracellular granule-rich area using holotomography. The proportion of lost cells after showing rupture-like events or membrane blebbing was higher in Day 2 37°C islets than in Day 2 24°C islets (0.35 ± 0.29% on Day 2 24°C vs. 12.41 ± 2.92% on Day 2 37°C, $p < 0.01$; Fig. 4D). The increase in the holotomography-defined cell loss fraction was directionally consistent with the lower viability and the higher proportion of terminal deoxynucleotidyl transferase (TUNEL)-positive cells observed in the Day 2 37°C group. Because these assessments were performed on different islets, the findings should be interpreted as group-level concordance rather than direct correlation. The intracellular granule-rich area was significantly lower in Day 2 37°C islets (21.64 ± 3.77% on Day 2 24°C vs 7.75 ± 2.29% on Day 2 37°C, $p < 0.01$; Fig. 4E). We also measured the GI of cytoplasm in both peripheral and central islet cells on Day 2 24°C and 37°C. GI was significantly lower in central than in peripheral islet cells under both culture conditions ($p < 0.001$ for 24°C, $p < 0.0001$ for 37°C; Fig. 4F). In comparison with Day 2 24°C islets, significant decrease was seen in cytoplasm in central islet cells on Day 2 37°C (73.67 ± 5.71 on Day 2 24°C vs. 37.93 ± 4.29 on Day 2 37°C, $p < 0.001$; Fig. 4F). Grayscale intensity ratio between central and peripheral cells also showed the similar tendency (0.70 ± 0.07 on Day 2 24°C vs. 0.37 ± 0.04 on Day 2 37°C, $p < 0.01$; Fig. 4G). Together, these data indicate that 37°C culture promotes central necrotic remodeling, cell death, and depletion of granule-rich structures, whereas 24°C culture preserves structural stability and granule-rich morphology.

Day 2 holotomographic changes might be associated with later in vitro functional impairment

Next, we evaluated whether early temperature-dependent morphological changes were associated with later functional outcomes in vitro. Islets were cultured for 14 days at 24°C or 37°C and analyzed according to the scheme in Fig. 5A. Day 14 24°C islets remained largely round and smooth, with few islet-to-islet adhesions and little central necrosis (Fig. 5B). Day 14 37°C islets more frequently showed fusion or aggregation and higher brightness. Hoechst 33342/PI staining revealed few dead cells in both groups at Day 14, suggesting that severely damaged cells or islets may have been lost during continued culture, leaving a selectively surviving islet population (Fig. 5B). The residual rate, defined as the percentage of islet number at each time point relative to that at the beginning of culture (Day 0), was significantly higher in 24°C cultures than in 37°C cultures over the observation period ($p = 0.013$; Fig. 5C). Viability at Day 14 remained high in both groups and did not differ significantly (Fig. 5D), whereas brightness, quantified as mean red-channel intensity, remained significantly higher in Day 14 37°C islets (118.02 ± 1.56 on Day 14 24°C vs. 141.14 ± 2.71 on Day 14 37°C, $p < 0.0001$; Fig. 5E).

Despite preserved viability, Day 14 37°C islets showed impaired endocrine function in vitro. GSIS under both low and high glucose conditions was significantly lower in Day 14 37°C islets than in Day 14 24°C islets (low glucose 0.43 ± 0.07 ng IEQ^{-1} h^{-1} in 24°C vs. 0.04 ± 0.01 ng IEQ^{-1} h^{-1} in 37°C, $p < 0.001$; high

glucose 0.59 ± 0.17 ng IEQ^{-1} h^{-1} in 24°C vs. 0.07 ± 0.02 ng IEQ^{-1} h^{-1} in 37°C, $p < 0.05$; Fig. 5F), whereas there was no significant difference in the stimulation index, defined as the ratio of insulin secretion under high and low glucose conditions (Fig. 5G). Insulin content per IEQ was also significantly lower in the 37°C group (64.77 ± 7.42 ng IEQ^{-1} vs. 27.68 ± 6.06 ng IEQ^{-1}, $p < 0.01$; Fig. 5H). Consistent with these functional data, expression of *Ins2* and *Sst* was markedly reduced in Day 14 37°C islets (*Ins2*: 1.03 ± 0.01 vs. 0.30 ± 0.03, $p < 0.0001$; Fig. 5I, *Sst*: 1.04 ± 0.01 vs. 0.12 ± 0.05, $p < 0.0001$; Fig. 5K). *Gcg*, *Pdx1*, and *Mafa* tended to be higher in Day 14 37°C islets, whereas *Nkx6.1* did not differ significantly (Fig. 5J, L–N). Among adhesion-related genes, *Itgb1* was significantly lower in Day 14 37°C islets (1.02 ± 0.01 vs. 0.70 ± 0.11, $p < 0.05$, Fig. 5P), whereas *Cdh1* and *Gjd2* were unchanged (Fig. 5O and Q).

We next performed RNA-seq analysis using extracted mRNA on Day 14 24 and 37°C islets from four independent islet isolations, each divided between the 24°C and 37°C culture conditions, yielding four biological replicates per condition. Figure 6A shows the principal component analysis (PCA) of these samples. Samples within the same group clustered closely, whereas samples from different groups showed distinct separation, suggesting condition-dependent differences in global gene expression profiles. PC1, PC2, and PC3 explained 55.2%, 9.3%, and 8.9% of the variance, respectively. Figure 6B shows differential gene expression patterns between Day 14 islets cultured at 24°C and 37°C. Upregulated genes in Day 14 37°C islets were associated with hypoxic stress and cell adhesion and extracellular matrix (ECM). By contrast, the apoptosis-related genes *Bcl2l14* and *Faim* were upregulated in Day 14 24°C islets. The expression of *Ins2* was attenuated, whereas genes associated with α-cell identity and islet differentiation were upregulated in Day 14 37°C islets. Furthermore, several genes were uniquely upregulated in Day 14 37°C islets. Some highly expressed genes in Day 14 37°C islets were also correlated with cell adhesion, extracellular matrix and cell death. *Postn* ($\log_2$ fold-change (logFC) 6.38, false discovery rate (FDR) < 0.001) encodes periostin, which acts as a ligand for integrin αVβ3 and αVβ5. *Spp1* (logFC 5.18, FDR < 0.001) encodes osteopontin, which promotes cellular proliferation and prevents apoptosis. NUPR1 (encoded by *Nupr1* (logFC 3.32, FDR < 0.001)) is a critical repressor of ferroptosis. Functional annotation clustering also revealed enrichment of cell adhesion- and ECM-related genes in Day 14 37°C islets (Fig. 6C).

Transplantation reveals a divergence between in vitro functional impairment and graft performance

Finally, we examined the transplantation performance of islets cultured for two weeks at 24°C or 37°C. Blood glucose after transplantation was transiently lower in the 24°C group (n = 10) during the first 3 days, whereas improved glycemic control in the 37°C group (n = 13) became evident by Day 7 ($p < 0.05$; Fig. 7A). Over the 28-day observation period, blood glucose was significantly lower in the 37°C group ($p = 0.034$; Fig. 7A). Plasma insulin increased after transplantation in both groups and was higher in the 37°C group, particularly on Day 14 ($p < 0.05$; Fig. 7B). Graft nephrectomy resulted in re-elevation of blood glucose and reduced plasma insulin in both groups (Fig. 7C and D), confirming graft-dependent endocrine function.

The normoglycemia rate was significantly higher in the 37°C group (20.0% vs. 69.2%, $p = 0.0145$; Fig. 7E). In the intraperitoneal glucose tolerance test, blood glucose was significantly lower in the 37°C group than in the 24°C group ($p = 0.023$; Fig. 7F), and the area under the curve was also lower ($p < 0.05$; Fig. 7G). Histological assessment demonstrated engrafted islets in both groups (Fig. 7H). These results reveal a divergence between functional impairment in vitro and graft performance in vivo.

Discussion

The present study demonstrates that label-free holotomography enables real-time 3D visualization of living islets and reveals dynamic injury patterns that are not captured by conventional bright-field microscopy. The main findings are threefold. First, islets cultured overnight, which are often assumed to be morphologically stabilized after isolation, retain dynamic vulnerability, including intercellular junction dissociation, rupture-like events, and membrane blebbing. Second, culture at 37°C induces central necrotic remodeling with extrusion of putative necrotic-core components, suggesting that central cavity formation is a dynamic process rather than a static endpoint. Third, these early holotomographic damage signatures are associated, at the culture-condition level, with later impairment of GSIS, insulin content, and endocrine gene expression in vitro. Together, these findings support the concept that islet deterioration follows spatially organized and dynamically evolving injury-associated morphological patterns.

One important observation was the detection of rupture-like and blebbing events in both central and peripheral regions of Day 0 islets. Central necrosis after isolation is typically attributed to hypoxia in the islet core.[6, 7] However, the presence of cell death at the periphery suggests that early post-isolation injury is not restricted to oxygen diffusion gradients. Isolation-related events such as enzymatic digestion, oxidative stress, extracellular matrix disruption, and loss of cell-matrix interactions can also contribute to islet cell apoptosis and dysfunction.[17, 18, 19] Plasma membrane rupture may reflect non-apoptotic cell death, including necrosis, necroptosis,[20] or pyroptosis,[21] whereas blebbing is a canonical morphological feature of apoptosis.[15, 16] Because holotomography does not provide molecular markers of cell-death pathways, these interpretations remain morphological. Nonetheless, the ability to visualize these events in real time provides a new window into the early dynamics of islet injury.

Intercellular junction dissociation in Day 0 islets was another unexpected finding. Overnight culture is commonly used to allow isolated islets to recover from the stress of collagenase digestion.[13, 22] However, holotomography revealed persistent instability of cell-to-cell cohesion in four of five Day 0 islets. This finding may reflect incomplete recovery of ECM and junctional structures after enzymatic digestion. The ECM and peri-insular matrix are known to contribute to islet integrity and isolation efficiency, and excessive digestion can promote islet fragmentation or cell dispersion, particularly in fragile species such as pigs.[23, 24, 25] Thus, holotomography may be useful for detecting residual structural vulnerability that is not apparent by conventional bright-field microscopy assessment.

The most distinctive Day 2 finding was central necrotic remodeling under 37°C culture. Oxygen tension falls sharply within the core of isolated islets, and oxygen availability and islet size are major determinants of islet survival.[7] Low-temperature culture can reduce metabolic demand and oxygen consumption, thereby limiting hypoxia-induced damage in mouse islets.[26] Consistent with this concept, 24°C culture preserved cell-to-cell cohesion and granule-rich features, whereas 37°C culture increased cell death, decreased granule density, and promoted central necrotic remodeling. Importantly, holotomography revealed extrusion of debris-like core components. This suggests that central cavities may form through dynamic core remodeling followed by reorganization or readhesion of peripheral cells, rather than through passive accumulation of dead cells. Because islets were imaged at their respective culture temperatures, the observed differences may reflect both accumulated culture-associated changes and acute temperature effects during imaging.

The relationship between early morphology and later function should be interpreted carefully. The Day 2 holotomographic measurements and Day 14 functional assays were performed on different islets; therefore, the data do not establish single-islet prediction. Instead, they show that culture conditions associated with early holotomographic damage are also associated with later impairment of GSIS, insulin content, and endocrine gene expression. These findings demonstrate culture-condition-level associations between early morphological changes and later in vitro function, without establishing predictive value for individual islets. Imaging the same individual islets longitudinally and then subjecting them to functional assays is warranted to establish true single-islet predictive power. Integration with automated image analysis or machine learning may further enable objective quality scoring for transplantation-oriented applications.

Finally, we discuss the discrepancy between functional impairment in vitro and superior graft performance in vivo in the 37°C group. Although 37°C culture induced early damage and reduced Day 14 insulin secretion in vitro, transplanted 37°C-cultured islets showed better glycemic control and higher normoglycemia rates. One possible explanation for the superior graft performance of the 37°C group is selection during prolonged culture. Islets with severe early injury may have been preferentially lost, as suggested by the lower residual islet rate, whereas the surviving islet population retained viability and the capacity to function after transplantation. Although individual islets were not followed longitudinally, these findings are compatible with culture-associated selection of surviving islets that retain transplantation potential. However, fusion or aggregation may also contribute to the reduced residual islet count, which therefore does not by itself establish selective loss of damaged islets. Because both groups received 200 IEQs, the transplantation experiments assessed the performance of equal IEQ doses of surviving cultured islets, rather than the total functional graft yield from an equivalent starting islet preparation. Additional processes, including engraftment efficiency, revascularization, host microenvironmental support, and adaptive stress responses, may also contribute to graft performance. Thus, in vitro functional assays and transplantation outcomes may reflect related but distinct biological dimensions of islet condition, and no single pretransplant assay is likely to predict graft outcome fully.

In conclusion, holotomography captures dynamic structural changes in living islets and provides complementary information for assessing islet condition alongside functional and transplantation-based measurements.

Methods

Study approval

The care of the mice and the experimental procedures complied with the Guide for the Care and Use of Laboratory Animals, 8th edition (National Research Council, 2011). The experimental protocol was approved by the Animal Care and Use Committee of Fukuoka University (approval number: 2407025).

Mouse islet isolation

Eight- to twelve-week-old male C57BL/6J mice (CLEA Japan, Tokyo, Japan) were used as syngeneic islet donors and diabetic recipients. Islets were isolated by collagenase digestion and density-gradient purification. Pancreatic tissue was digested at 37°C for 18 min using 1 mg mL^{-1} collagenase V (catalog No. C9263; Merck/Sigma-Aldrich, St. Louis, MO, USA) solution. Then, the islets were isolated using Ficoll PM70 (catalog No. F2878; Merck/Sigma-Aldrich) at density gradients of 1.100, 1.083, 1.077, and 1.040 and centrifugation at 840 *g* for 13 min. Approximately 100% purity was achieved using a 70 μm Cell Strainer (catalog No. 431751; Corning Inc., Corning, NY, USA) and handpicking under a microscope.

Culture conditions and grouping

Isolated islets were cultured in low-glucose DMEM (catalog No. 11885-084; Thermo Fisher Scientific/Gibco, Waltham, MA, USA) containing 10% fetal bovine serum and 1% antibiotics overnight under an atmosphere of 5% CO_2 at 24°C. After that, they were cultured in the same medium at 24°C or 37°C for two days or two weeks.

Residual rate of cultured islets

Cultured islets were counted on Day 0 (the day after overnight culture), 2, 5, 8, and 14. The number of islets on Day 0 was set at 20. The residual rate was calculated as the percentage of islets remaining at each time point relative to the Day 0 count.

Viability of islet cells

Islet cell viability was measured on Day 0, 2 and 14. Islets were stained with Hoechst 33342 (catalog No. H3570; Thermo Fisher Scientific/Invitrogen, Waltham, MA, USA) and propidium iodide (PI; catalog No. P1304MP; Thermo Fisher Scientific/Invitrogen) to detect nuclei and dead cells, respectively. Viability was calculated as ([Hoechst 33342-positive cells] − [PI-positive cells]) ÷ [Hoechst 33342-positive cells] × 100 (%).

Imaging of cultured islets using conventional bright-field microscopy

Images of cultured islets were obtained at ×400 magnification using Z-stack mode with 3.5-μm intervals on a BZ-X700 microscope (Keyence, Itasca, IL, USA) for comparison with holotomography. Images captured at ×100 magnification were used to assess mean islet intensity. Intensity measurements were performed using ImageJ software (https://imagej.nih.gov/ij/index.html; National Institutes of Health, Bethesda, MD, USA). Color information was split into red, green, and blue channels, and the mean intensity was calculated from the red-channel image.

Label-free holotomography

Holotomographic analyses included five islets per condition obtained from 1 islet isolation. Measurements from multiple optical sections and sampling locations were averaged within each islet. Real-time holotomographic imaging of cultured islets (Day 0, Day 2 at 24°C and 37°C) was performed using the HT-X1 system (Tomocube, Daejeon, Republic of Korea). Imaging was performed using an objective lens numerical aperture (NA) of 0.95, a condenser lens NA of 0.72, and an illumination wavelength of 450 nm. The imaging volume measured 165 μm × 165 μm × 62 μm. One entire islet was imaged within each field of view. Time-lapse images were captured for 1–2 h under the corresponding culture temperature in an incubator (24 or 37°C). The interval of capturing images was 2 minutes. Islet cell loss (%) was calculated as the number of cells lost during the observation period (1h) divided by the number of cells present at the start of imaging, multiplied by 100. The granule-rich area fraction was defined as the percentage of the islet cross-sectional area occupied by pixels with a grayscale intensity of 255. Cell loss and the granule-rich area fraction were assessed in three optical sections at the upper, middle, and lower levels of each islet and averaged to obtain one value per islet. Absolute RI data were not retained; therefore, quantitative RI analysis was not performed. Instead, GIs ranging from 0 to 255 were measured in the exported 8-bit TIFF images using ImageJ. Five locations were sampled within each compartment—granule-like structures, peripheral cytoplasm, and central cytoplasm—and averaged to obtain one value per compartment per islet. The central-to-peripheral intensity ratio was calculated for each islet by dividing its mean central intensity by its mean peripheral intensity. The quantification was done using Image J software (ImageJ 1.53t; https://imagej.nih.gov/ij/index.html; National Institutes of Health, Bethesda, MD, USA).

Measurement of glucose-stimulated insulin secretion of cultured islets

GSIS was assessed on Day 14 islets. Ten islet equivalents (IEQs, 1 IEQ is defined as an islet with a 150-μm diameter) were placed into a transwell insert (Millicell Hanging Cell Culture Insert PET 8.0um, 24-well; catalog No. MCEP24H48, Merck/Millipore, Burlington, MA, USA) and preincubated in 1 mL of 3.3 mM (60 mg dL^{-1}) glucose solution for 60 min. After removal of the supernatant, inserts were sequentially transferred to another 1 mL of 3.3 mM glucose solution (low glucose) and then to 16.5 mM

glucose solution (300 mg dL^{-1}, high glucose) and incubated for 60 min under each condition. All preincubation and glucose-stimulation steps were performed at 37°C for both culture groups. Supernatants were collected for insulin measurement using an ELISA kit (LBIS Mouse Insulin ELISA Kit, catalog No. 292-89401; Fujifilm Wako/Shibayagi, Shibukawa, Japan) according to the manufacturer's instructions.

Measurement of the insulin content of cultured islets

Insulin content in Day 14 islets was measured after extraction from 10 IEQs using 1 mL of RIPA buffer (catalog No. 22352-04; Nacalai Tesque, Kyoto, Japan) containing a protease and phosphatase inhibitor mix (catalog No. 04080-24 and catalog No. 07575-51; Nacalai Tesque). Insulin content (defined as the total amount of insulin in 1 IEQ) was measured using an LBIS Mouse Insulin ELISA Kit (Fujifilm Wako/Shibayagi) and expressed per IEQ.

RNA extraction and cDNA synthesis

Before performing quantitative reverse transcription polymerase chain reaction (qRT-PCR), islets from four independent isolations were divided between the 24°C and 37°C culture conditions. RNA was extracted from approximately 500 IEQs on Day 14 using 1 mL TRIzol Reagent (catalog No. 15596026; Thermo Fisher Scientific/Invitrogen) and purified using a PureLink RNA Mini Kit (catalog No. 12183018A; Thermo Fisher Scientific/Invitrogen) according to the manufacturer's instructions. RNA concentrations were measured using a NanoDrop 2000 spectrophotometer (catalog No. ND-2000; Thermo Fisher Scientific). Complementary DNA (cDNA) was synthesized using extracted RNA using a QuantiTect Reverse Transcription Kit (catalog No. 205311; Qiagen, Tokyo, Japan).

Real-time reverse transcription polymerase chain reaction analysis

qRT-PCR was performed using a CFX Connect Real-Time PCR Detection System (Bio-Rad Laboratories, Hercules, CA, USA) and Thunderbird SYBR qPCR Mix (catalog No. QPS-101; Toyobo, Osaka, Japan). Primers are listed in Supplemental Table 1 and were designed by Takara Bio (Kusatsu, Japan). Relative quantitation was performed using LightCycler software version 4.1, and the results were normalized to a reference gene (*Actb*). The data are presented as fold differences, calculated using the $2^{-\Delta\Delta Ct}$ method.

RNA sequencing

RNA-seq was performed using islets from four independent isolations. Islets from each isolation were divided between the 24°C and 37°C culture conditions, yielding four biological replicates per condition. RNA was extracted from cultured islets (Day 14 24 and 37°C islets) and purified as described above. RNA sequencing libraries were prepared from 1 μg of RNA using a TruSeq Stranded mRNA LT Sample Prep Kit (catalog No. 20020595; Illumina), according to the manufacturer's instructions. Cluster amplification and 151-bp paired-end sequencing were performed in accordance with the manufacturer's protocol for the NovaSeq (Illumina).

RNA was sequenced by Cell Innovator (Fukuoka, Japan). Raw data read quality was analyzed using FastQC version 0.11.7 (http://bioinformatics.babraham.ac.uk/projects/fastqc/). Quality trimming and adapter clipping were performed using Trimmomatic version 0.38:[27] trailing bases were trimmed if below a quality score of 15, to a minimum length of 36 bases, and Illumina adapters were removed. Trimmed reads were mapped to transcripts in the reference data for *Mus musculus*/GRCm38 using the Bowtie2 aligner within RNA-Seq by Expectation-Maximization (RSEM).[28] The abundance of both genes and isoforms was estimated using RSEM in transcripts per million (TPM) counts.

Differentially expressed genes (DEGs) were identified using the edgeR program.[29] Normalized counts per million values, $\log_2$ fold-changes (logFC), and false discovery rate FDR were obtained from the gene-level TPM counts. The criteria for DEGs were FDR ≤ 0.05 and ratios of ≥ 2-fold for up- and downregulated genes.

Induction of diabetes in recipient mice

Diabetes was induced in recipient mice by intravenous injection of streptozotocin (180 mg kg^{-1} body mass, catalog No. S0130; Merck/Sigma-Aldrich). Mice with blood glucose concentrations > 400 mg dL^{-1} were used as diabetic recipients.

Islet transplantation

Recipient diabetic mice were anesthetized using 1.5% isoflurane. After anesthesia was achieved, the left kidney was mobilized through a dorsal skin incision, and 200 IEQs were infused into the left renal subcapsular space using Gastight Syringes 1002 RN (Hamilton, Reno, NV, USA) with Intramedic polyethylene tubing (0.58 mm, catalog No. BD427410; Becton Dickinson, Franklin Lakes, NJ, USA).

Assessment of the function of transplanted islets

The function of the transplanted islets was assessed by monitoring blood glucose and plasma murine insulin concentrations for 28 days after transplantation. Normoglycemia was defined as a blood glucose concentration of < 200 mg dL^{-1}. Plasma murine insulin concentrations were measured using an LBIS Mouse Insulin ELISA Kit (Fujifilm Wako/Shibayagi). An intraperitoneal glucose tolerance test (GTT) was performed after > 10 h fasting by intraperitoneal injection of 2 g kg^{-1} glucose solution. Blood glucose was measured at 0 (before glucose stimulation), 30, 60, 90, and 120 min after injection, and the area under the curve, defined as blood glucose (mg dL^{-1}) × time after glucose injection (min), was also calculated.

Histological and immunofluorescence analyses of cultured islets

Pancreatic islets cultured at either 24°C or 37°C for 2 days were collected and embedded in agarose. Agarose-embedded islets were then fixed in 10% neutral buffered formalin and embedded in paraffin. Serial sections (4-μm thick) were prepared using a microtome. For histological evaluation, sections were

stained with hematoxylin and eosin (H&E). Multiplex immunofluorescence staining was performed to detect apoptotic islet cells. After deparaffinization and rehydration, apoptotic cells were detected using the Click-iT Plus TUNEL Assay for In Situ Apoptosis Detection with Alexa Fluor 647 (catalog No. C10619; Thermo Fisher Scientific/Invitrogen, Waltham, MA, USA) according to the manufacturer's instructions. Subsequently, insulin immunostaining was performed using a prediluted guinea pig anti-insulin (catalog No. A056401-2, RRID AB_2617169; Agilent, Dako, Tokyo, Japan) as the primary antibody. After incubation with the primary antibody, Alexa 488-conjugated donkey anti-guinea pig (catalog No. 715-547-003, RRID AB_2340472; 1:100; Jackson ImmunoResearch Laboratories) was used as the secondary antibody. Nuclear counterstaining and mounting were performed using ProLong Gold antifade mountant with DAPI (catalog No. P36935; Thermo Fisher Scientific/Invitrogen, Waltham, MA, USA). Images were obtained using a BZ-X700 microscope (Keyence, Itasca, IL, USA). The percentage of apoptotic islet cells was calculated as the number of TUNEL-positive nuclei divided by the total number of DAPI-positive nuclei in islets.

Histological and immunofluorescence analyses of engrafted islets

The left kidney was recovered one month after transplantation. Recovered kidneys were fixed using 10% formalin solution, embedded and sectioned at 3-μm thickness. Sections were stained with H&E or immunohistochemically for insulin and Ki67. Primary antibodies used were prediluted guinea pig anti-insulin (catalog No. A056401-2, RRID AB_2617169; Agilent, Dako, Tokyo, Japan), rabbit anti-insulin (catalog No. ab181547, RRID AB_2716761; 1:1,000; Abcam, Cambridge, UK) and rabbit anti-Ki67 antibody (catalog No. ab66155, RRID AB_1140752; 1:200; Abcam). After incubation with the primary antibody, Alexa 488-conjugated donkey anti-guinea pig (catalog No. 715-547-003, RRID AB_2340472; 1:100; Jackson ImmunoResearch Laboratories) and Cy3-conjugated goat anti-rabbit (catalog No. 111-165-144, AB_2338006; 1:100; Jackson ImmunoResearch Laboratories) were used as secondary antibodies. Nuclei were stained with 4',6-diamidino-2-phenylindole (DAPI, catalog No. 340–07971; Dojindo). Images were obtained using a BZ-X700 microscope (Keyence, Itasca, IL, USA), and immunostaining was quantified using ImageJ software.

Statistics and Reproducibility

Blood glucose, plasma insulin, GTT data and residual rate of cultured islets were analyzed using a repeated-measures model with culture group as the between-subject factor and time as the within-subject factor. Within-subject effects were evaluated using multivariate F tests (Supplementary Tables 2–5). Time to the first attainment of normoglycemia was analyzed using the Kaplan–Meier method and compared between groups using a two-sided log-rank test. Mice that did not achieve normoglycemia were censored at their last observation. Comparisons between two groups were performed using a two-tailed Student's t-test (viability, apoptotic cell, lost islet cells, granule-rich area of islet, central-to-peripheral grayscale intensity ratio, GSIS, stimulation index, insulin content, PCR data, brightness, blood glucose and plasma insulin after graftectomy and AUC of blood glucose). Multiple

comparisons were performed using a one-way analysis of variance (ANOVA) with post-hoc Tukey test (GI). Data are presented as mean ± standard error of the mean. A two-sided $p < 0.05$ was defined as significant. Statistical analyses were conducted using JMP19.1.3 (SAS Institute, Cary, NC, USA).

Declarations

Acknowledgements

We thank Ms. Yuriko Hamaguchi for her assistance with islet cell culture and Mr. Takuya Matsui and Mr. Kazuki Yamaguchi in SHINKO SEIKI Co., Ltd. for capturing images of holotomography. During the preparation of this manuscript, the authors used ChatGPT 6.0 thinking by OpenAI to assist with English language editing and improving the clarity of the text. The authors reviewed and edited all AI-assisted content and take full responsibility for the final content of the manuscript. Weblio web dictionary (https://ejje.weblio.jp/) was also used for checking English words. We thank Robin James Storer, PhD, from Edanz (https://jp.edanz.com/ac) for editing drafts of this manuscript.

Data availability

The datasets used and/or analyzed in the present study are available from the corresponding author upon reasonable request.

Ethics approval

Animals were housed under specific pathogen-free conditions with free access to food and water. The care of the animals and the experimental procedures complied with the Guide for the Care and Use of Laboratory Animals, 8th edition (National Research Council, 2011). The experimental protocol was approved by the Animal Care and Use Committee of Fukuoka University (Approval number: 2407025). This study was reported in accordance with the ARRIVE guidelines. All experiments were performed in accordance with relevant guidelines and regulations.

Authorship

NS planned the study, performed all the experiments and data analyses except the histological assessment, and wrote the first draft of the manuscript. RK performed histological assessments and revised the draft of the manuscript. TY and GY revised the manuscript. SK supported the study design and revised the draft of the manuscript. NS and SK are the guarantors of the work, and as such, take responsibility for the contents of the article. All authors read and approved the final manuscript.

Disclosure

The authors declare no conflicts of interest.

Funding

The present study was funded by an intramural grant from Fukuoka University (No. GR2420, to NS), the Japan Diabetes Foundation and Sanofi K.K. (No. 240434 to NS), Takahashi Industrial and Economic Research Foundation (No. 250038 to NS), and a Grant-in-Aid for Scientific Research “KAKENHI” (No. 25K11992, to NS, and No. 24K02514, to SK).

References

1. Vantyghem, M.-C., de Koning, E.J.P., Pattou, F., Rickels, M.R.: Advances in β-cell replacement therapy for the treatment of type 1 diabetes. Lancet. **394**, 1274–1285 (2019)
2. Papas, K.K., et al.: Islet Oxygen Consumption Rate (OCR) Dose Predicts Insulin Independence in Clinical Islet Autotransplantation. Plos One. **10**, e0134428 (2015)
3. Kato, H., et al.: Biological hypoxia in pre-transplant human pancreatic islets induces transplant failure in diabetic mice. Sci. Rep. **14**, 12402 (2024)
4. Bertuzzi, F., Ricordi, C.: Prediction of Clinical Outcome in Islet Allotransplantation. Diabetes Care. **30**, 410–417 (2007)
5. Ricordi, C., Lakey, J.R.T., Hering, B.J.: Challenges toward standardization of islet isolation technology. *Transplantation Proceedings* 33, 1709 (2001)
6. Giuliani, M., et al.: Central Necrosis in Isolated Hypoxic Human Pancreatic Islets: Evidence for Postisolation Ischemia. Cell Transplant. **14**, 67–76 (2005)
7. Komatsu, H., et al.: Oxygen environment and islet size are the primary limiting factors of isolated pancreatic islet survival. PLoS One. **12**, e0183780 (2017)
8. Sakata, N., Yoshimatsu, G., Kawakami, R., Aoyagi, C., Kodama, S.: Optimal temperature for the long-term culture of adult porcine islets for xenotransplantation. Front. Immunol. **14**, 1280668 (2023)
9. Medina-Ramirez, I.E., Macias-Diaz, J.E., Masuoka-Ito, D., Zapien, J.A.: Holotomography and atomic force microscopy: a powerful combination to enhance cancer, microbiology and nanotoxicology research. Discov Nano. **19**, 64 (2024)
10. Park, Y., Depeursinge, C., Popescu, G.: Quantitative phase imaging in biomedicine. Nat. Photonics. **12**, 578–589 (2018)
11. Sandoz, P.A., Tremblay, C., van der Goot, F.G., Frechin, M.: Image-based analysis of living mammalian cells using label-free 3D refractive index maps reveals new organelle dynamics and dry mass flux. PLoS Biol. **17**, e3000553 (2019)
12. D'Brant, L.Y., Desta, H., Khoo, T.C., Sharikova, A.V., Mahajan, S.D., Khmaladze, A.: Methamphetamine-induced apoptosis in glial cells examined under marker-free imaging modalities. J. Biomed. Opt. **24**, 1–10 (2019)
13. Corbin, K.L., West, H.L., Brodsky, S., Whitticar, N.B., Koch, W.J., Nunemaker, C.S.: A Practical Guide to Rodent Islet Isolation and Assessment Revisited. Biol. Proced. Online. **23**, 7 (2021)
14. Steer, S.A., Scarim, A.L., Chambers, K.T., Corbett, J.A.: Interleukin-1 stimulates beta-cell necrosis and release of the immunological adjuvant HMGB1. PLoS Med. **3**, e17 (2006)

15. Paluch, E.K., Raz, E.: The role and regulation of blebs in cell migration. Curr. Opin. Cell Biol. **25**, 582–590 (2013)
16. Ortega-Carrion, A., Feo-Lucas, L., Vicente-Manzanares, M.: Cell Migration. In: Encyclopedia Cell. Biology) (2016)
17. Paraskevas, S., Maysinger, D., Wang, R., Duguid, T.P., Rosenberg, L.: Cell loss in isolated human islets occurs by apoptosis. Pancreas. **20**, 270–276 (2000)
18. Thomas, D.A., et al.: Mitochondrial targeting with antioxidant peptide SS-31 prevents mitochondrial depolarization, reduces islet cell apoptosis, increases islet cell yield, and improves posttransplantation function. J. Am. Soc. Nephrol. **18**, 213–222 (2007)
19. Bottino, R., et al.: Response of human islets to isolation stress and the effect of antioxidant treatment. Diabetes. **53**, 2559–2568 (2004)
20. Degterev, A., et al.: Chemical inhibitor of nonapoptotic cell death with therapeutic potential for ischemic brain injury. Nat. Chem. Biol. **1**, 112–119 (2005)
21. Fink, S.L., Cookson, B.T.: Caspase-1-dependent pore formation during pyroptosis leads to osmotic lysis of infected host macrophages. Cell. Microbiol. **8**, 1812–1825 (2006)
22. Carter, J.D., Dula, S.B., Corbin, K.L., Wu, R., Nunemaker, C.S.: A practical guide to rodent islet isolation and assessment. Biol. Proced. Online. **11**, 3–31 (2009)
23. Sakata, N., Yoshimatsu, G., Kawakami, R., Chinen, K., Aoyagi, C., Kodama, S.: Procedure of Adult Porcine Islet Isolation. Tissue Eng. Part. C Methods. **29**, 144–153 (2023)
24. van Deijnen, J.H., Hulstaert, C.E., Wolters, G.H., van Schilfgaarde, R.: Significance of the peri-insular extracellular matrix for islet isolation from the pancreas of rat, dog, pig, and man. Cell. Tissue Res. **267**, 139–146 (1992)
25. Kim, H.I., et al.: Parameters for successful pig islet isolation as determined using 68 specific-pathogen-free miniature pigs. Xenotransplantation. **16**, 11–18 (2009)
26. Itoh, T., et al.: Low temperature condition prevents hypoxia-induced islet cell damage and HMGB1 release in a mouse model. Cell. Transpl. **21**, 1361–1370 (2012)
27. Bolger, A.M., Lohse, M., Usadel, B.: Trimmomatic: a flexible trimmer for Illumina sequence data. Bioinformatics. **30**, 2114–2120 (2014)
28. Li, B., Dewey, C.N.: RSEM: accurate transcript quantification from RNA-Seq data with or without a reference genome. BMC Bioinform. **12**, 323 (2011)
29. Robinson, M.D., McCarthy, D.J., Smyth, G.K.: edgeR: a Bioconductor package for differential expression analysis of digital gene expression data. Bioinformatics. **26**, 139–140 (2010)

Figures

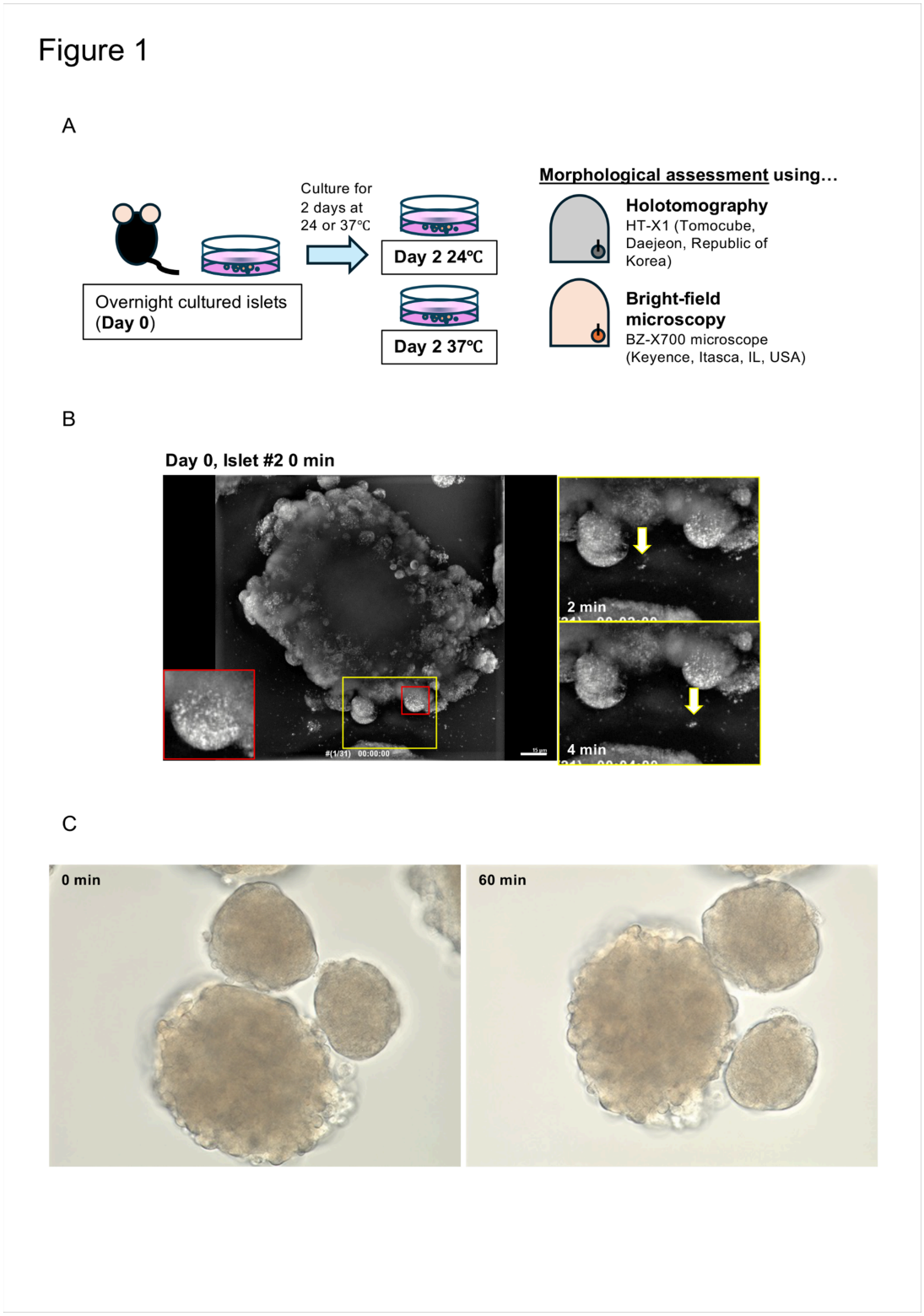

Figure 1

Study design and visualization of living islets by label-free holotomography

A. Scheme of this study. Islets isolated from C57BL/6J mice were cultured overnight at 24°C (Day 0) and then cultured for two additional days at either 24°C or 37°C (Day 2 24°C and Day 2 37°C). Islets on Day 0, Day 2 24°C, and Day 2 37°C were imaged by label-free holotomography and conventional bright-field

microscopy. B. Holotomographic image of No. 2 islet on Day 0 (Figure S2). The red square indicates a region of a single endocrine cell. Yellow arrows indicate high-intensity granule-like structures released from an islet cell (yellow circle). The scale bar represents 15 μm. C. Bright-field microscopic image of an islet on Day 0 at the start of observation (0 min) and after 60 min. Images were captured using a Z-stacking technique. The original magnification was ×400.

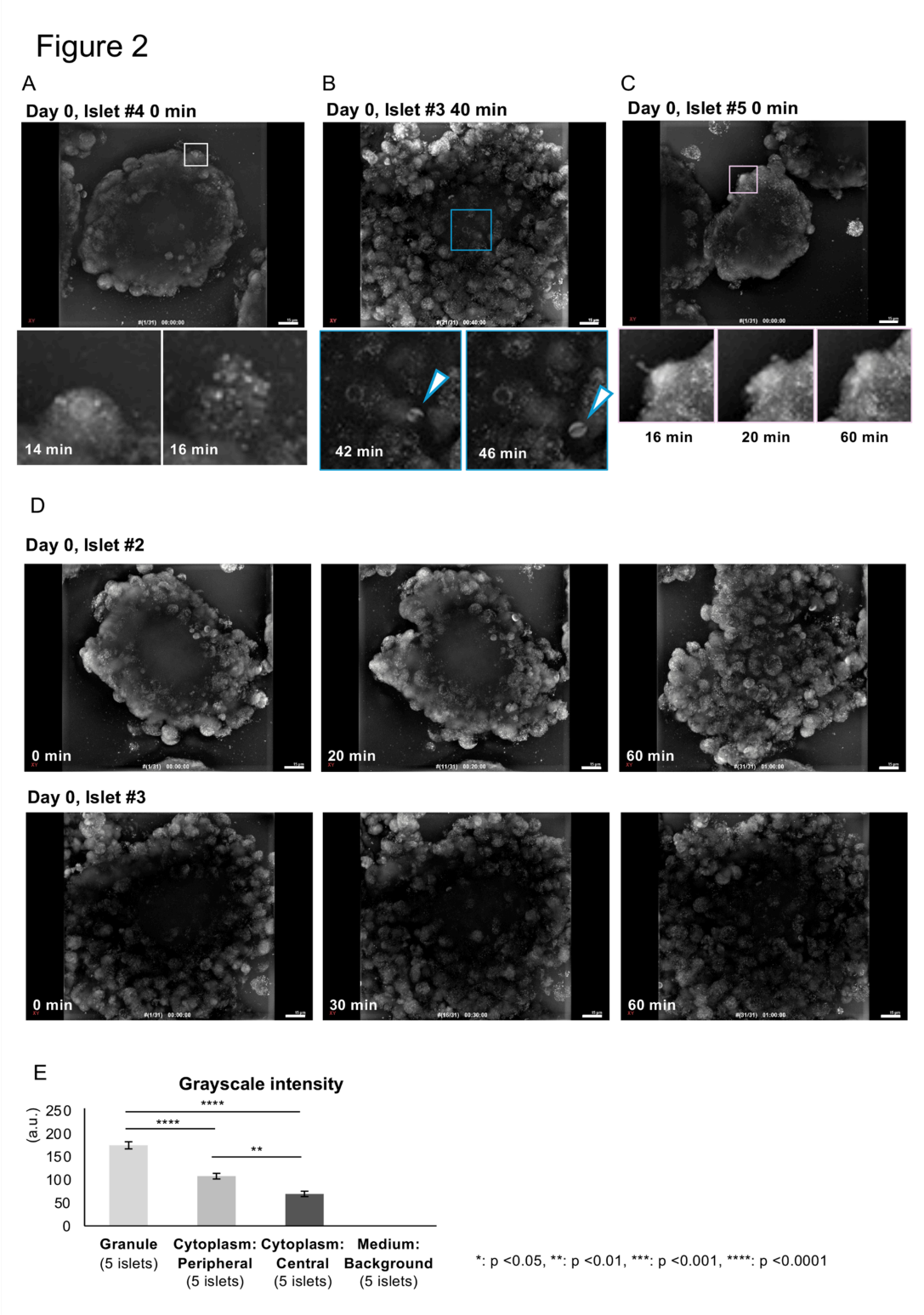

Figure 2

Holotomography reveals early cell-death-like events and intercellular junction dissociation in Day 0 islets

A and B. Representative images of rupture-like non-apoptotic cell-death events. A. Holotomographic image of No. 4 islet on Day 0. The cell indicated by the white square expanded at 14 min from the beginning of observation and ruptured at 16 min. B. Holotomographic image of No. 3 islet on Day 0. The blue square indicates the ruptured cell. A nuclear or nuclear-remnant-like structure (triangle) appeared at 42 min. C. Representative blebbing event in No. 5 islet on Day 0. The purple square indicates a blebbing cell. D. Representative intercellular junction dissociation in No. 2 (left) and No. 3 (right) islets on Day 0 (Supplementary Figures 2 and 3). The scale bar represents 15 μm. E. Grayscale intensity of each intracellular components including granule-like structures (Granules), cytoplasm in peripheral islet cells (Cytoplasm: Peripheral) and cytoplasm in central islet cells (Cytoplasm: Central). As a negative control, grayscale intensity in medium (Medium: Background) was included in the graph. Differences with $p < 0.05$ were considered significant.

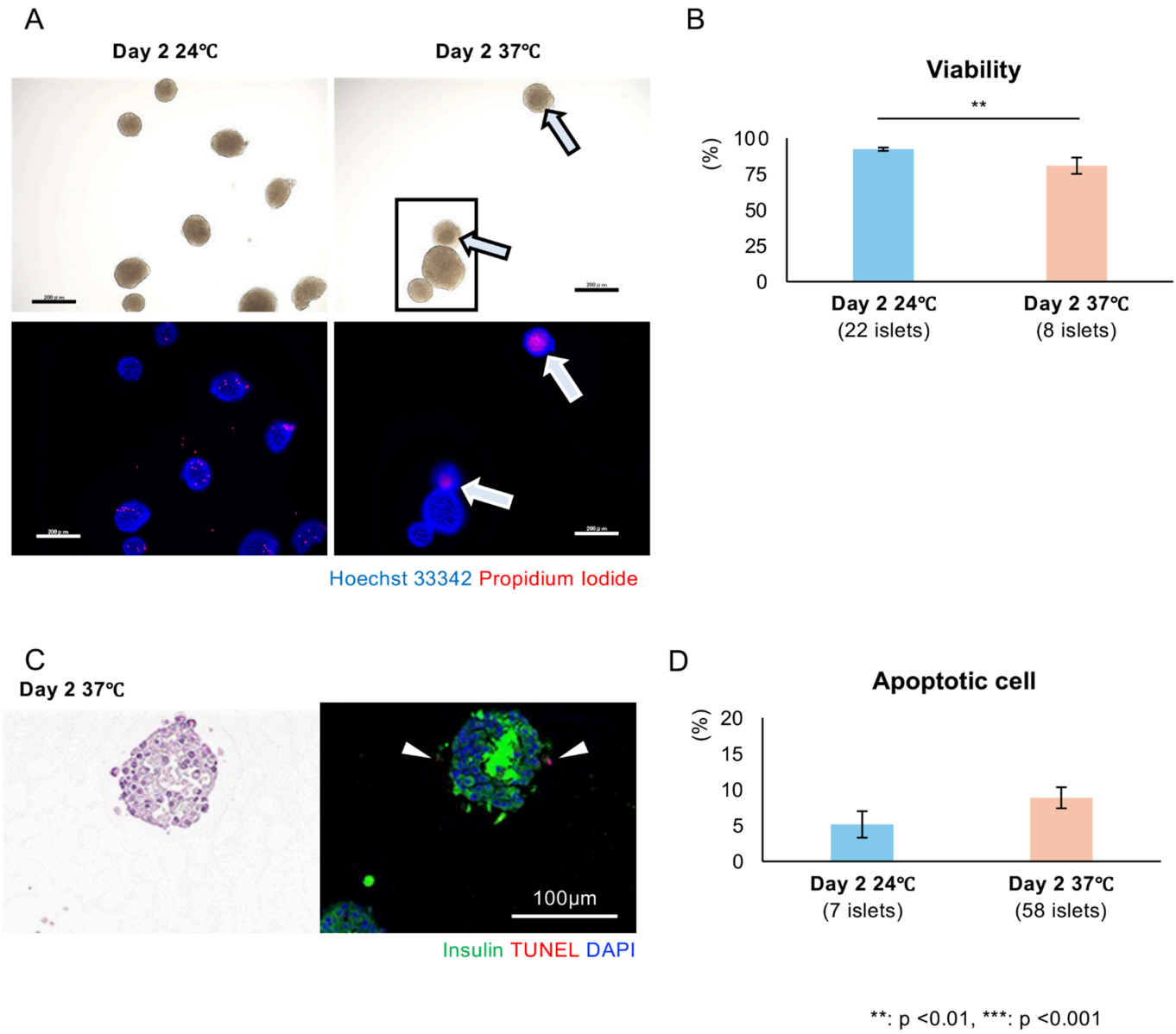

Figure 3

Morphological characteristics of cultured islets on Day 2

A. Unlabeled images and Hoechst 33342/propidium iodide-stained images of Day 2 islets cultured at 24°C or 37°C. The scale bar represents 200 μm. B. Viability of islet cells on Day 2 24°C (left, light blue) and 37°C (right, light orange). C. Hematoxylin and eosin staining and fluorescence images of islets on Day 2 at 37°C showing central necrosis (left) and TUNEL-positive apoptotic cells (right). Green indicates

insulin immunoreactivity, red indicates TUNEL-positive cells, and blue indicates nuclei. D. Percentage of apoptotic islet cells on Day 2 24°C (left, light blue) and 37°C (right, light orange). Data are presented as mean ± standard error of the mean. Differences with $p < 0.05$ were considered significant.

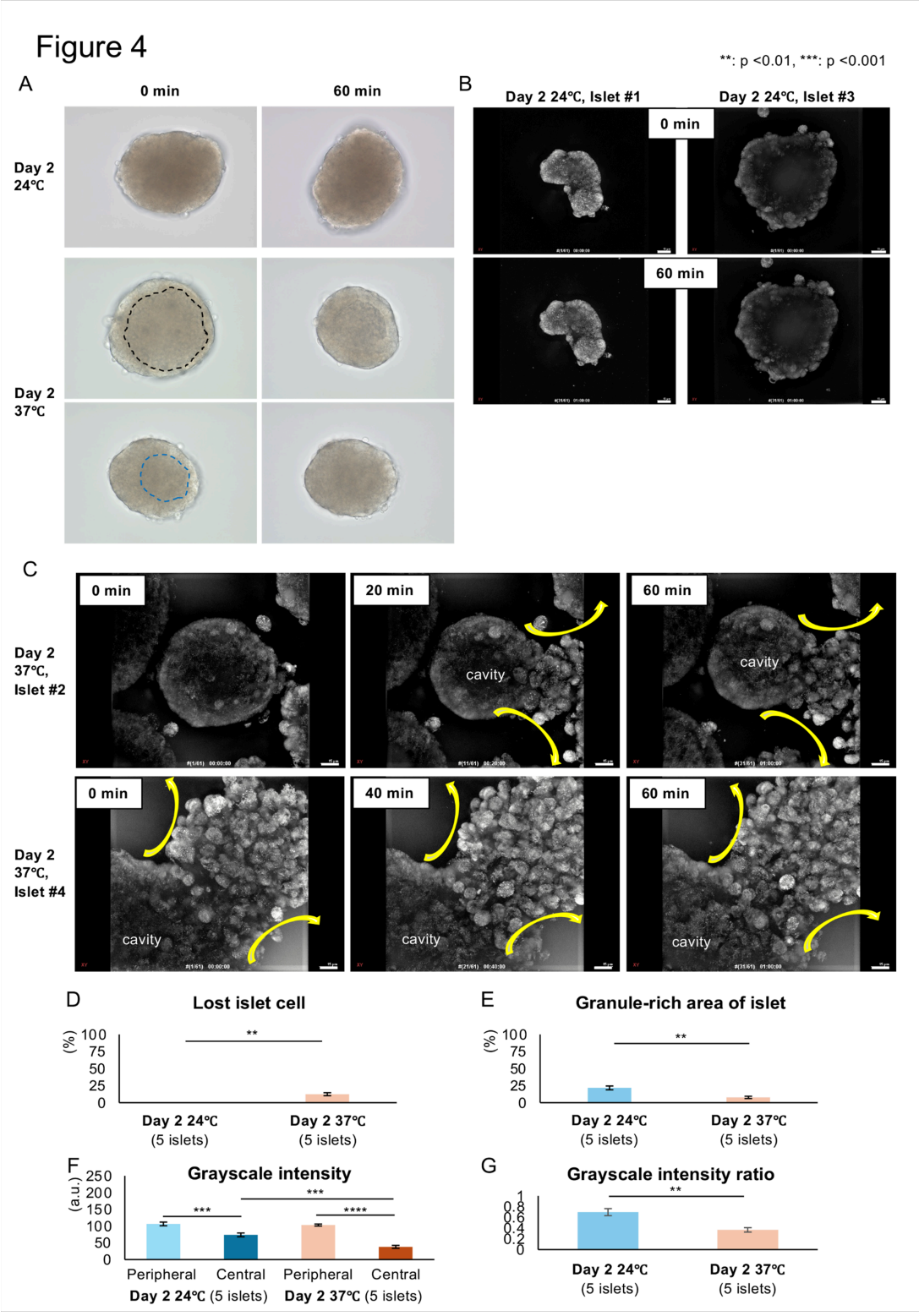

Figure 4

Holotomography reveals temperature-dependent central necrotic remodeling of pancreatic islets

A. Bright-field microscopic image of an islet on Day 2 24°C and 37°C. The dotted black line indicates the central cavity, and the blue line indicates necrosis. Images were captured using a Z-stacking technique at ×400 magnification. B. Holotomographic image of No. 1 and 3 islets on Day 2 24°C (Figures S6 and 8, respectively). C. Holotomographic image of No. 2 and No. 4 islets on Day 2 37°C (Figures S12 and 14, respectively). Yellow arrows indicate extrusion of central necrotic components. The scale bar represents 15 μm. D and E. Percentage of lost islet cells (D) and granule-rich area of islet cells (E) on Day 2 24°C and 37°C. F. Grayscale intensity in peripheral and central islet cells on Day 2 24°C and 37°C. G. Central-to-peripheral grayscale intensity ratio in Day 2 islets cultured at 24°C or 37°C. Holotomographic images were used for quantification. Data are presented as mean ± standard error of the mean. Differences with $p < 0.05$ were considered significant.

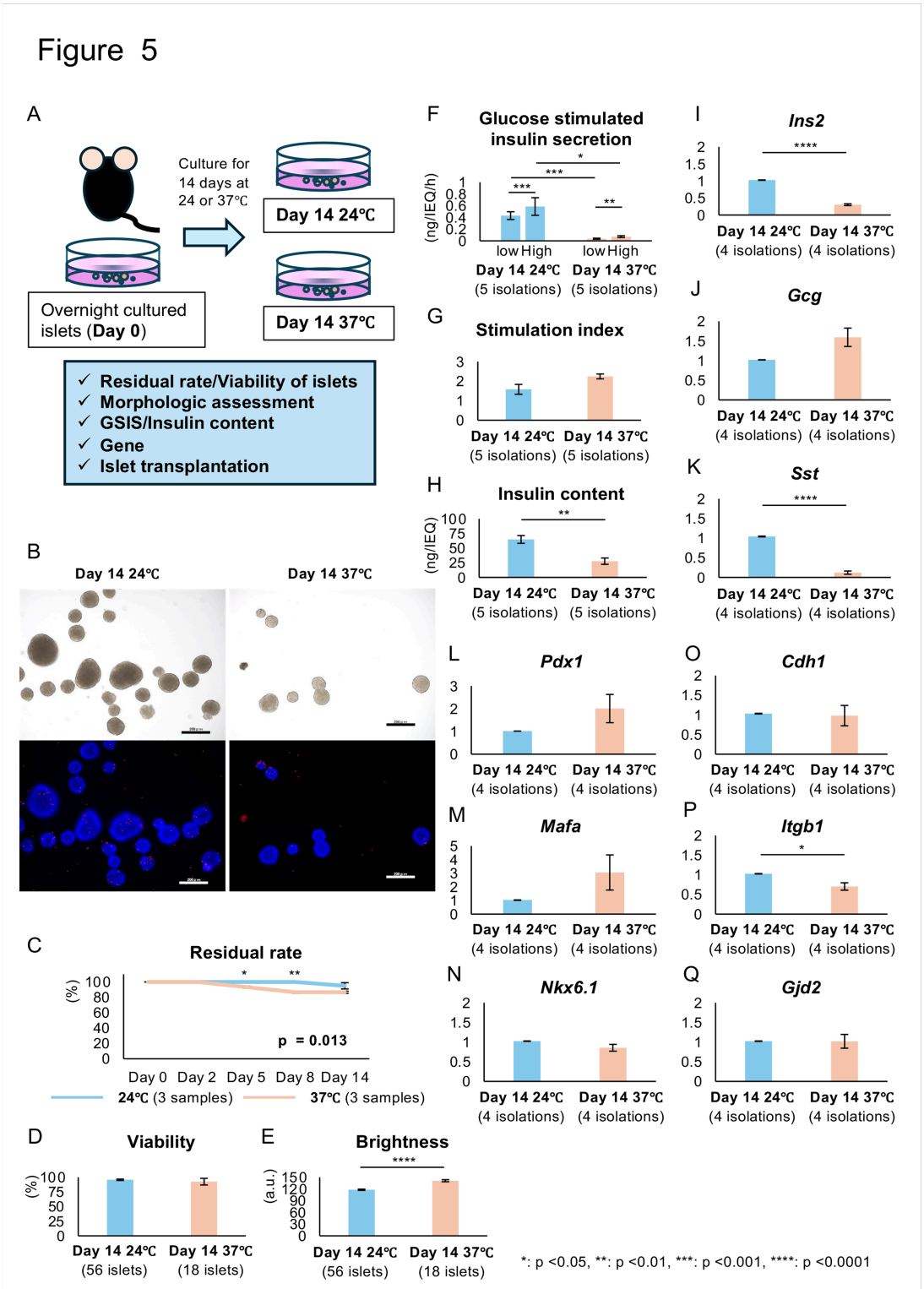

Figure 5

Functional assessments of islets on Day 14

A. Scheme of the Day 14 experiments. Islets isolated from C57BL/6J mice were cultured overnight at 24°C (Day 0) and then cultured for 14 days at 24°C or 37°C. Islets were used for residual rate and viability measurements, morphological assessment using bright-field microscopy, glucose-stimulated insulin

secretion, insulin content measurement, qPCR analysis, and syngeneic islet transplantation using diabetic C57BL/6J mice. B. Unlabeled images and Hoechst 33342/propidium iodide-stained images of islets on Day 14 at 24°C and 37°C. The scale bar represents 200 μm. C. Residual rate of islets cultured at 24°C (light blue) and 37°C (light orange) on Day 2, 5, 8, and 14. D and E. Viability (D) and brightness, quantified as mean red-channel intensity, (E) of islets on Day 14 24°C (light blue) and 37°C (light orange). F–H. Glucose-stimulated insulin secretion (F), stimulation index (G) and insulin content per IEQ (H) of Day 14 24°C (light blue) and 37°C (light orange). I–Q. Gene expression in islets on Day 14 as assessed by qPCR: endocrine function (*Ins2*, I; *Gcg*, J; *Sst*, K), islet development (*Pdx1*, L; *Mafa*, M; *Nkx6.1*, N), and adhesion factors (*Cdh1*, O; *Itgb1*, P; *Gjd2*, Q). Data are presented as mean ± standard error of the mean. Differences with $p < 0.05$ were considered significant.

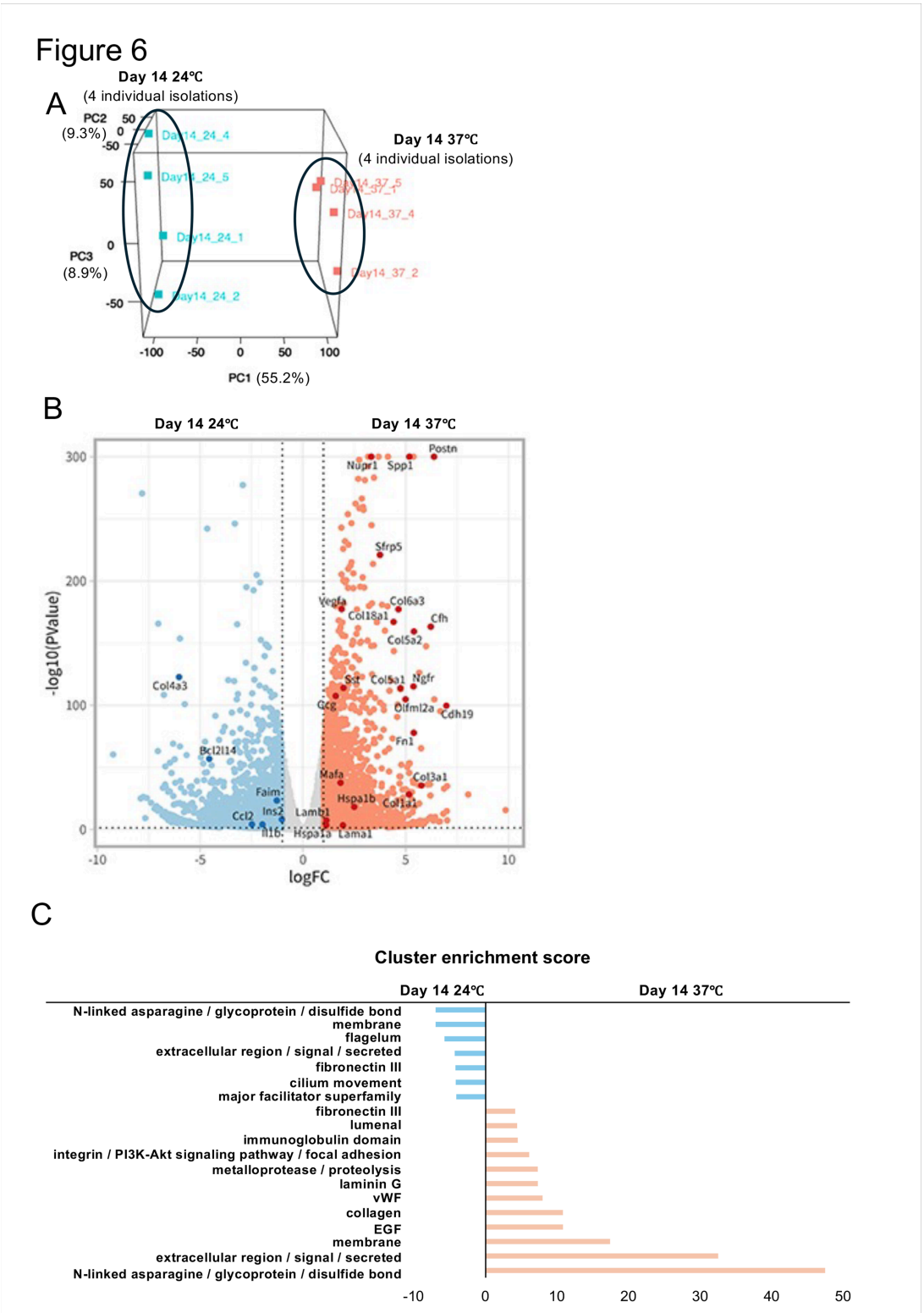

Figure 6

RNA-seq of islets on Day 14 at 24°C or 37°C

A. PCA plot showing the overall distribution of islet samples from 4 islet isolations based on normalized gene expression profiles. Each point represents a sample from one of four independent islet isolations. Islets from each isolation were divided between the two culture conditions (blue: 24°C, orange: 37°C).

The percentages on the axes indicate the proportion of variance explained by PC1, PC2 and PC3. B. Volcano plot of expressed genes. Blue, highly expressed genes on Day 14 24°C; orange, highly expressed genes on Day 14 37°C. $|Log_2$ fold-change (logFC)| ≥ 1 is defined as highly expressed. C. Functional annotation clustering. Clusters with enrichment scores ≥4 are shown. Blue: highly expressed cluster on Day 14 24°C, Orange: highly expressed cluster on Day 14 37°C.

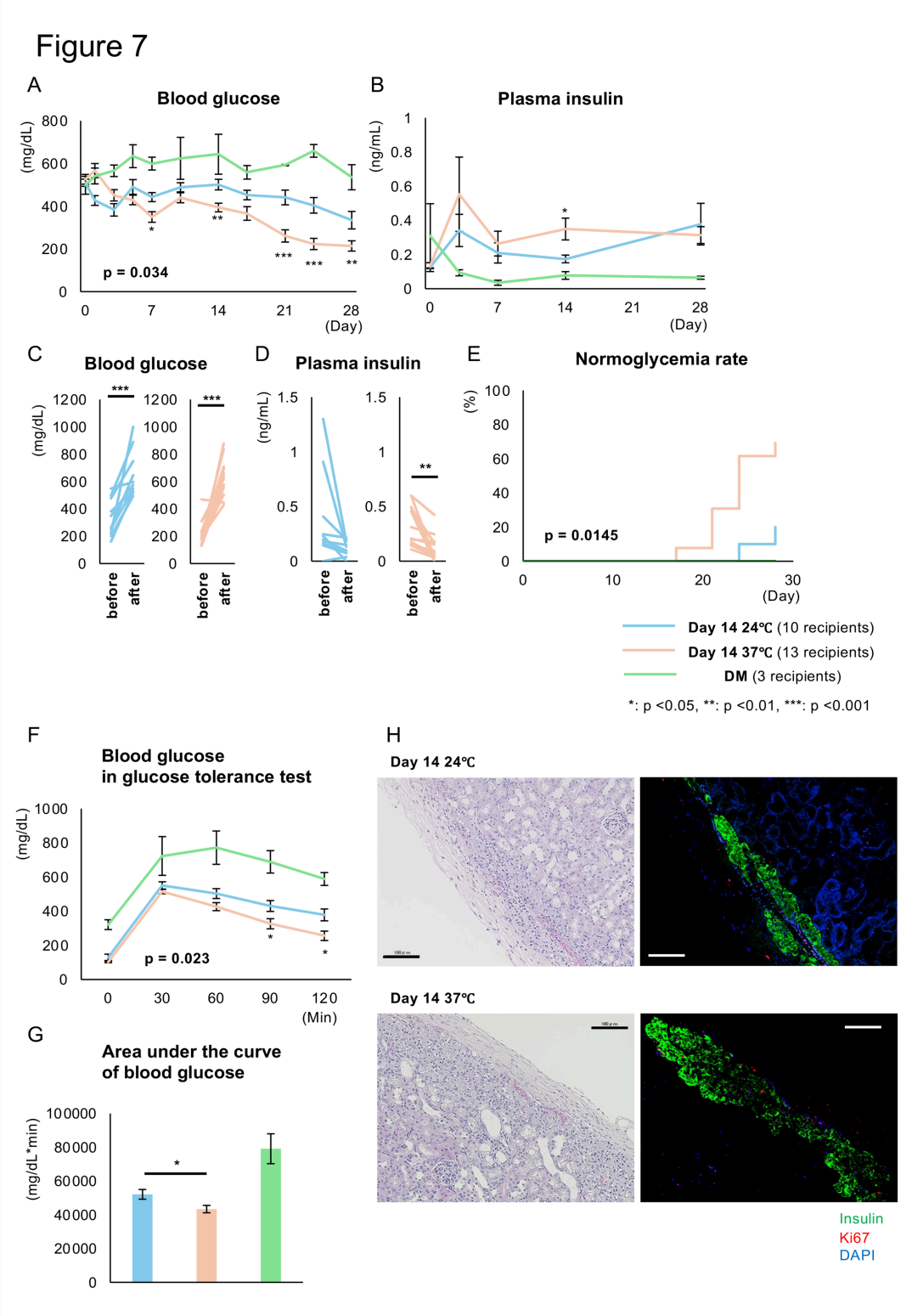

Figure 7

Transplantation of Day 14 islets cultured at 24°C or 37°C

A and B. Blood glucose concentrations (A) and plasma insulin concentrations (B) after islet transplantation. C and D. Blood glucose concentrations (C) and plasma insulin concentrations (D) before and after graft nephrectomy. E. Normoglycemia rate after islet transplantation. F and G. Blood glucose concentrations (F) and area under the curve (G) in the intraperitoneal glucose tolerance test 28 days after transplantation. Light blue, Day 14 24°C group; light orange, Day 14 37°C group; light green, DM group. H. Islet graft 28 days after transplantation: upper panel, Day 14 24°C group; lower panel, Day 14 37°C group. The scale bar represents 100 μm. Data are presented as mean ± standard error of the mean. Differences with $p < 0.05$ were considered significant.

Supplementary Files

This is a list of supplementary files associated with this preprint. Click to download.

- SupplementalInformationComBiol.pdf
- VideoS3Day237C2h.mp4
- VideoS2Day224C2h.mp4
- VideoS1Day0overnight.mp4